

# Temporal Variations of Mid-IR Spectra in Late-Type Stars

J. D. Monnier<sup>1</sup>, T. R. Geballe<sup>2</sup>, and W. C. Danchi<sup>1</sup>

## ABSTRACT

New multi-epoch, mid-infrared (8-13  $\mu\text{m}$ ) spectrophotometric observations are presented for 30 late-type stars. The observations were collected over a four year period (1994-1997), permitting an investigation of the mid-infrared spectral shape as a function of the pulsation cycle (typically 1-2 years). The spectra of stars with little excess infrared emission and those with carbon-rich dust show the least spectral variability, while stars with evidence for dusty, oxygen-rich envelopes are most likely to show discernible variations in their spectral profile. Most significantly, a large fraction of variable stars with strong 9.7  $\mu\text{m}$  emission features show clear spectral profile changes which repeat from one cycle to the next. The significant sharpening of the silicate feature near maximum light can not be fully explained by heating and cooling of the circumstellar dust shell during the pulsational cycle, suggesting that the dust optical properties themselves must also be varying. In addition, the appearance of a narrow emission feature near the silicate peak for a few stars may require the production of especially “pure” silicate dust near maximum light. The general narrowing of the silicate feature observed may reflect the evolution of the pre-existing dirty grains whose surface impurities have been evaporated off when the grain temperature rises preceding maximum light. An improved theory of dust formation which can explain the observed changes in the grain properties around a single, pulsating star may lead to a definitive explanation for the diversity of silicate emission profiles observed amongst oxygen-rich, late-type stars.

*Subject headings:* stars: AGB and post-AGB, stars: circumstellar matter, stars: mass-loss, stars: variables, ISM: dust

## 1. Introduction

The mid-infrared (8-13  $\mu\text{m}$ ) spectra of late-type stars have been measured by many observers since the development of infrared detectors. These red giants and supergiants are often surrounded by dusty envelopes which absorb stellar radiation and re-radiate the energy in the near- and mid-infrared. The infrared spectra can be classified based on the chemical content of the circumstellar environment (oxygen- or carbon-rich) and on the optical thickness of the dusty envelope (e.g., Merrill & Stein 1976a,b). Oxygen-rich circumstellar environments often produce spectra evincing a feature near 9.7  $\mu\text{m}$  resulting from the presence of silicate dust (Woolf & Ney 1969). This feature appears in emission for optically thin envelopes or in absorption when large enough optical depths are encountered. The emission spectra of dust surrounding carbon stars are nearly featureless, although often containing an 11.3  $\mu\text{m}$  feature attributed to SiC. In addition, many of these red giants and supergiants are classified as long-period variables, pulsating with a typical period of 1-2 years.

---

<sup>1</sup>Space Sciences Laboratory, University of California, Berkeley, Berkeley, CA 94720-7450

<sup>2</sup>Joint Astronomy Centre, 600 North A’ohoku Place, University Park, Hilo, HI 96720

The homogeneous set of survey measurements by the Infra-Red Astronomical Satellite (IRAS) in the mid-1980s allowed observers to classify silicate emission features based on various schemes (IRAS Science Team 1986; Little-Marenin & Little 1988, 1990; Goebel et al. 1989; Sloan & Price 1995). The different shapes of the feature have been interpreted largely as due to differences in the chemical make-up of oxygen-rich dust. Unfortunately the IRAS program did not conscientiously include observations of the mid-infrared spectra of long-period variable stars at different phases of their luminosity cycles, and there are only a few cases where such data have been retrieved from the IRAS Low Resolution Spectrometer (LRS) database. These observations have suggested silicate feature strength variations as a function of pulsational cycle, but have been hampered by limited temporal coverage (Little-Marenin, Stencel, & Staley 1996). More recent results by Creech-Eakman et al. (1997) point towards evidence for variations in the silicate feature as a function of pulsational phase, but the comparison spectra were taken nearly a decade apart. Hence, the simple observational question of whether the mid-infrared spectra of LPVs change shape through the pulsational cycle has been left without a decisive answer.

A campaign of observations taken from 1994 to 1997 was designed to monitor the mid-infrared spectrum of nearly 30 late-type stars. The observations, sampling the spectrum of most stars multiple times within a pulsational cycle, used the same instrument and observing technique. The homogeneity of this data set is important for allowing reliable spectral comparisons, avoiding complicating issues such as different apertures and calibration methods. This paper presents the full data set collected thus far and discusses the spectral variability (or lack of variability) of our sample stars.

## 2. Observations

Mid-infrared spectrophotometry was carried out with the United Kingdom Infra-Red Telescope (UKIRT) from 1994 to 1997. These observations employed the 32-element, linear array spectrometer CGS3 and were obtained with a 5" diameter aperture and standard chopping and nodding techniques. Wavelength calibrations were derived from observations of a krypton arc lamp in 4th, 5th, and 6th order, and are accurate to  $\pm 0.02 \mu\text{m}$ . The wavelength resolution of the observations was  $\sim 0.2 \mu\text{m}$ , sampled three times per resolution element. Flux calibrations were derived from observations of  $\alpha$  Lyr,  $\alpha$  Aur,  $\alpha$  CMa, and other bright standard stars. All standard stars used for ratioing are of spectral type K0 or earlier, so that absorption in the fundamental band of SiO, which is very prominent in late K and M giants and supergiants, is minimal in the ratioed spectra and does not affect the shapes of the reduced spectra.

The uncertainty in the *absolute* flux level was determined from the internal consistency of an intercomparison of photometric standards observed on a given night. Specific determinations of the uncertainty for individual nights, along with other observing information, can be found in Table 1. Note that for spectra taken on 1994 November 20, which was not photometric, the uncertainty is probably  $\pm 20\%$ .

Intracomparison of spectra from stars with little dust emission taken on different nights ( $\alpha$  Boo,  $\delta$  Oph, etc.) indicates the *relative* flux calibration within a single spectrum to be accurate to about one percent. Details of the spectral shape are least reliable near  $9.7 \mu\text{m}$ , due to strong telluric absorption by ozone. Inspection of the entire data set reveals the relative calibration for 1997 March 17 to be less accurate than the others, occasionally showing a 5-15% miscalibration longward of  $12 \mu\text{m}$  presumably due to changing telluric H<sub>2</sub>O absorption. It is important to refer to Table 1 when judging the quality of an individual spectrum.

### 3. Results

The observed stars were divided into three categories after inspecting the full set of spectra. Figure 1 shows spectra from 18 stars whose mid-infrared spectral shapes showed no apparent changes during our observing campaign; this includes stars which were observed only a single time ( $\beta$  Peg, Egg Nebula, and U Her). Figure 2 contains spectra from 8 stars whose  $9.7\ \mu\text{m}$  silicate feature show clear enhancement over the stellar/dust continuum during maximum light. Lastly, there are 4 stars which belong to neither of the above groups and these spectra can be found in Figure 3. These stars show either a change in the mid-infrared spectral slope or increased rms fluctuations in the spectral shape.

Figures 1-3 all share the same format. The upper panels show the full set of calibrated data, while the lower panels display the relative spectra for each source as determined by the following method. First, normalized spectra are produced by dividing each spectrum by its mean flux between  $8\text{--}13\ \mu\text{m}$  and then are smoothed ( $\Delta\lambda = 0.2\ \mu\text{m}$ ). Then, after removing spectra with known calibration problems (1997 March 17 observations and the cloudy data from 1994 August 26, see Table 1), the set of normalized spectra for each star is averaged together to form a mean spectral shape. Finally, this mean spectrum is divided into each of the normalized spectra to produce plots of the deviation from the cycle-averaged spectral shape, which are displayed in the lower panels. The rms fluctuation about the mean spectral shape is calculated for each star and is denoted by  $\sigma$  each lower panel. Spectra deemed unreliable are not included here and thus the bottom panel is absent if our observations lacked a sufficient number of “clean” spectra (at least two).

In addition, each panel contains a legend which tabulates the mean  $8\text{--}13\ \mu\text{m}$  fluxes in Janskys, the dates of observation, and the pulsation cycle phases, where applicable. Table 2 contains the pulsational characteristics, mostly drawn from the recently released Hipparcos Catalog (ESA 1997), along with spectral type and the number of spectra presented in this work. A few stars which are classified as semiregulars have their pulsational phases included only if a very recent phase determination is available (e.g., VX Sgr and W Hya). Each date of observation is assigned its own linestyle for all figures to facilitate intercomparisons between different stars and different nights. The vertical scale of the bottom panels is fixed so the relative magnitude of the spectral shape variations within this sample can be easily accessed. Although the data presented here do not have adequate temporal coverage to justify a detailed analysis of the light curves, inspection confirms the earlier finding that the infrared maximum is generally about  $\Delta\phi \approx 0.1$  after the optical maximum for Mira variables (Lockwood & Wing 1971).

#### 3.1. “Constant” Stars

Figure 1 contains the observations of stars whose spectra showed no discernible shape changes during this campaign. Some of these stars are both spectrally constant and show little excess infrared radiation, justifying their traditional role as calibrators for spectral observations. In particular,  $\alpha$  Boo,  $\alpha$  Her,  $\alpha$  Tau, and  $\delta$  Oph are among the most spectrally constant of all objects observed, and were used to infer the true calibration uncertainty in this survey. Only stars having spectral shape variations less than 2.0% rms and no overall slope changes were selected to be included as “constant” stars. Note again that the 1994 August 26 absolute photometry for  $\alpha$  Boo,  $\alpha$  Sco, and  $\delta$  Oph is not reliable due to clouds (see Table 1).

Of all the strongly variable stars with clear  $9.7\ \mu\text{m}$  silicate features included in this survey, only NML Cyg appears to possess a constant spectral shape in this wavelength regime. Despite a significant change in flux during this campaign ( $\sim 0.25$  magnitudes), the spectral shape is remarkably constant. By considering multi-wavelength photometric and interferometric measurements, Monnier et al. (1997) estimated the  $11\ \mu\text{m}$

optical depth to be about 2; hence, it is not surprising that the spectral shape hardly changes, since the dust at the  $\tau_{\text{mid-IR}} = 1$  surface lies far enough away from the star as to not to be strongly affected by its varying luminosity. These same arguments apply for the relatively flat mid-IR spectrum of VY CMa, whose optical depth at  $11\ \mu\text{m}$  has also been estimated to be  $\gtrsim 2$  (Danchi et al. 1994; Le Sidaner & Le Bertre 1996). Be reminded, however, that interpretations of present interferometric data is subject to change, since most of it has implicitly assumed spherical symmetry. The situation is further complicated for VY CMa, because it’s mid-IR spectrum has apparently recently undergone a dramatic change. About 25 years ago, Merrill & Stein (1976a,b) observed this silicate feature to be in strong emission (similar in strength to VX Sgr), and we can not offer an explanation for its “disappearance.”

The University of California at Berkeley Infrared Spatial Interferometer (ISI) survey of the  $11\ \mu\text{m}$  angular sizes of late-type stars (Danchi et al. 1994) detected two stars whose dust shells were quite distant from the stellar surface ( $R_{\text{dust}} \gtrsim 40R_{\star}$ ),  $\alpha$  Ori and  $\alpha$  Sco. While no firm conclusions can be drawn for  $\alpha$  Sco due to a lack of “clean” spectra, sufficient high-quality  $\alpha$  Ori spectra were available to conclude that its mid-infrared spectral shape was constant to within error bars. This constancy is consistent with the interferometric observations, which suggest the dust is located far from the star, relatively immune to the effects of stellar variability. However, a recent report (Bester et al. 1996) indicates a fresh dust formation episode around  $\alpha$  Ori, contributing  $\sim 10\%$  of the  $11\ \mu\text{m}$  flux. Modest changes in this hot dust spectrum during our campaign of observations would not be definitively detected within our experimental uncertainty since the flux from the cool, distant dust shell dominates the mid-IR dust emission.

By inspecting the deviations from the cycle-averaged spectral shapes (the bottom panels of Figure 1), one can see many bumps and dips resulting from miscalibration. No firm conclusion in this paper has been based on any fluctuations which are both small (few percent) and not correlated with the pulsational phase (or flux) of the star. These fluctuations limit the precision to which the peak of the spectral features can be measured and should be not interpreted beyond the uncertainty implied by these observations of standard stars.

In summary, stars with weak silicate features or no features at all are most likely to show no spectral shape variations. In addition, not one carbon stars in our sample (CIT 6, IRC +10216, or V Hya) showed an overall change of spectral shape or variation in the strength of the SiC feature during a luminosity cycle (refer to §3.3 for IRC +10216 spectra). For some O-rich stars, mid-infrared interferometric observations exist to correlate little spectral variability with either high dust shell opacity or the presence of a dust shell far from the central star ( $R_{\text{dust}} \gtrsim 40R_{\star}$ ).

### 3.2. Silicate Feature Variation

The most interesting results of this paper are found in Figure 2, in which data are presented for 8 stars which exhibit systematic spectral changes directly related to the pulsational phase. It is worth noting that a large fraction of the surveyed stars with a distinct  $9.7\ \mu\text{m}$  feature are in this category. Two different types of spectral shape variability are observed: an overall narrowing of the silicate feature near maximum light seen in most of the stars and a more narrow emission feature near the peak of the silicate feature seen only for a few sources. Even CIT 3, whose spectrum reveals a dusty envelope with optical depth only slightly smaller than that for NML Cyg (as judged by the partial self-absorption of the silicate feature), shows the same systematic shape changes as for stars with optically thin envelopes (e.g., *o* Cet and U Ori).

The certain identification of the spectral changes as related to the pulsational phase is confirmed in two

different ways. First, the reality of this effect is attested to by the large number of stars which show the sharpening of the  $9.7\ \mu\text{m}$  silicate feature near maximum. There is no case where the silicate peak is seen to grow relative to the dust emission in the wings (near  $12\ \mu\text{m}$ , for example) at the minimum of the luminosity cycle. A second way to positively correlate the spectral changes with the flux output of the star is to obtain spectra at the same phase or flux level, but one pulsational period apart. In cases where this proved possible ( $\chi$  Cyg, CIT 3, IK Tau,  $o$  Cet, and U Ori), the spectral shapes showed convincing agreement. For example, U Ori showed a relatively flat silicate feature after one luminosity minimum, developing a peakier feature at maximum. Further data taken after the following minimum showed again a flattened dust spectrum, while a final observation taken at  $\phi = 0.01$  revealed a peaked spectrum similar to that observed one cycle earlier.

This effect appears to have been first observed by Forrest, Gillett, & Stein (1975, hereafter FGS75), but was not connected to the pulsational phase. While a total of six  $o$  Cet mid-IR spectra spanning a 6 year period were presented, only the first observation occurred sufficiently near maximum to show silicate enhancement. The other observations all showed significantly less silicate emission, leading FGS75 to speculate that the infrared excess around this star was decreasing slowly over time. The data presented here clearly favors an interpretation which links the amount and character of the silicate emission to the phase of  $o$  Cet.

The evolution of the silicate enhancement from luminosity minimum to maximum could not be continuously followed for a few sources (R Aqr and VX Sgr) due to inadequate temporal coverage. In these cases it is possible that the silicate enhancement may have occurred suddenly, and/or may not repeat from one cycle to the next. This is especially pronounced for VX Sgr which shows a strong, narrow enhancement near maximum ( $\phi = 0.84$ ). The most recent measurement,  $\phi = 0.85$  on 1997 August 29, may be starting to show a  $9.7\ \mu\text{m}$  enhancement, but further data at the end of 1997 is necessary to determine if this feature re-appears and can indeed be associated with the pulsational cycle.

In order to investigate the physical mechanisms responsible for the spectral changes, further analysis of the spectral shapes was performed on a subset of the stars with the most complete temporal coverage. On this basis, the spectra of IK Tau, U Ori, and  $o$  Cet were chosen to represent the entire data set in subsequent analysis. CIT 3 was excluded because its mid-IR spectrum suggests that the dust shell is optically thick. These stars show the silicate feature enhancement quite strongly and it is expected that the physical mechanism or mechanisms responsible for the spectral changes in these sources should apply to the others.

Subtracting the “stellar component” from the spectrum allows the changes in the dust spectrum to be seen more clearly. The stellar spectrum is approximated as a 2500 K blackbody and is fitted to the  $8\ \mu\text{m}$  datum in the mid-IR spectrum (Little-Marenin & Little 1990). The “stellar-subtracted” spectra for IK Tau, U Ori, and  $o$  Cet are found in Figure 4. All three sources show a relative increase in the  $9.7\ \mu\text{m}$  feature relative to the dust emission in the wings (near  $12\ \mu\text{m}$ , for example) which appears near the maximum. This is clear just by visual inspection, since the dust emission at  $12\ \mu\text{m}$  changes usually by less than a factor of 2, while the peak flux varies by more than a factor of 2. In addition, U Ori shows a spectrally narrow ( $\sim 0.5\ \mu\text{m}$ ) feature near the silicate peak arising near maximum light. While this feature is only apparent for U Ori in Figure 4, the narrow character of the  $\chi$  Cyg and R Aqr silicate emission near maximum (seen in Figure 2) may be of a similar nature.

### 3.2.1. Appearance of “Pure” Silicates near Maximum Luminosity

While the relatively large increase in 8-11  $\mu\text{m}$  flux as compared to 11-13  $\mu\text{m}$  flux can be partially attributed to the dust shell temperature increase during maximum light, we will show that the large magnitude of the observed changes implies that the dust optical constants themselves are changing. Furthermore, the narrow emission feature of U Ori is clearly of non-thermal origin; the Planck function has no such narrow features. This is strong evidence that much of the mid-IR emission near maximum light comes from relatively pure silicate dust particles, as judged by the general narrowing of the silicate peak and, in the case of U Ori, by the extreme sharpness of the 9.7  $\mu\text{m}$  resonance. Such pure silicates may be formed from pre-existing, “dirty” grains which are “purified” via grain surface evaporation of metal impurities or re-crystallization of amorphous grains during the temperature rise towards maximum light (Tielens 1990; Stencel et al. 1990; Dominik, Sedlmayr, & Gail 1993). Alternatively, the dirty silicates formed at minimum light may be destroyed leaving only small dust grains to emit their distinctive spectrum (Little-Marenin et al. 1996). The lack of the narrow U Ori feature in the IK Tau and *o* Cet spectra could be due to different shell geometries, different chemical abundances, or peculiarities of recent pulsational cycles.

### 3.2.2. Constructing the Color-Color Diagram

Although the qualitative changes in the spectral shapes are plain to see, it is useful to connect with previous studies of the silicate emission feature. A recent classification scheme which is easy to implement yet reproduces many of the important features of earlier work is given by Sloan & Price (1995, hereafter SP95). SP95 construct a color-color diagram to define a one-parameter family of the mid-IR spectral shapes. Following Creech-Eakman et al. (1997), the SP95 procedure was further simplified by using a 2500 K Planck function as an approximate stellar spectrum and fitting it to the flux at 8  $\mu\text{m}$  (as described above). Figure 5 was produced from the data found in Figure 4.

SP95 define the “spectral emission index,” which varies from SE1 to SE8, to parameterize the solid curve, beginning at  $\frac{F_{10}}{F_{11}} = .5$  to  $\frac{F_{10}}{F_{11}} = 1.4$  (see Figure 5 of SP95); the dividing lines are located on Figure 5. The optical constants of Draine & Lee (1984) and Ossenkopf, Henning, & Mathis (1992), two dust optical property models commonly used in radiative transfer calculations, describe the 9.7  $\mu\text{m}$  spectral signature of amorphous silicate dust, a signature which places these spectra with spectral emission indices SE5 to SE8. SP95 further identify spectra classified as SE4 to SE6 with spectra containing 10 and 11  $\mu\text{m}$  emission components, thought to be produced by warm crystalline olivine (Little-Marenin & Little 1990; Sloan & Price 1995). Although not relevant to the spectra in this paper, the lower-left portion of the SP95 color-color diagram is reserved for mid-infrared spectra which are very broad (SE1 to SE3), thought to originate from alumina grains (Onaka, de Jong, & Willems 1989; Sloan & Price 1995). Because of the difficulty in matching the data in Figure 5 with the corresponding pulsational phases, we have plotted the spectral emission index as a function of pulsational phase in Figure 6.

The data from IK Tau, U Ori, and *o* Cet can be seen to span a continuous range on the SP95 color-color diagram (see Figure 5), starting at SE4 and ending with SE7. While useful for classifying the general shapes of silicate features, one can not expect the SP95 color-color diagram to fully describe the mid-infrared spectral shape since only 3 discrete wavelengths are sampled, i.e. the narrow U Ori emission feature observed in this study would not have a strong signature in Figure 5. Figure 6 makes it clear that the silicate feature variations are in phase with the pulsational cycle, showing high spectral emission index values near maximum light and significantly lower values just after minimum.

A variety of effects can cause changes in the spectral emission index as a function of stellar luminosity. Variations in the optical depth or temperature of the dust could cause each star’s location on the SP95 color-color diagram to shift, especially if self-absorption is occurring at the peak of the silicate feature. The phase-dependent evolution of the dust optical constants responsible for changes in the SP95 spectral emission index in Figures 5 and 6 may be related to the narrow emission feature seen for U Ori. The following sections explore these possibilities in more detail.

### 3.2.3. *Dust Self-Absorption*

If the temperature profile and optical properties of the dust shell remain unchanged, then overall changes in the optical depth will not cause a shift in the SP95 spectral emission index if the dust envelope remains optically thin. The Infrared Spatial Interferometer (ISI) has obtained mid-IR visibility data for IK Tau, *o* Cet, and U Ori, and were fit, along with IRAS-LRS spectra, by circumstellar dust shell models assuming a spherically symmetric outflow (Danchi et al. 1994). These models indicate  $11\ \mu\text{m}$  optical depths of  $\sim 1.7$ ,  $\sim 0.1$ , and  $\sim 0.1$  for IK Tau, *o* Cet, and U Ori respectively. Hence, the optically thin condition is expected to hold for *o* Cet and U Ori, but not for IK Tau. This explains the more rounded nature of silicate feature for IK Tau and its lower spectral emission index, consistent with self-absorption at the peak of the silicate feature.  $\chi$  Cyg, R Aqr, and VX Sgr were also observed and modeled by the ISI, resulting in estimated  $11\ \mu\text{m}$  optical depths of 0.43, 0.23, and 0.56 respectively. Hence, optical depth effects are not expected to explain the spectral shape changes observed in most of the stars in Figure 2 which show silicate feature enhancement near maximum light.

One would think that optical depth effects would be important for CIT 3 (see Figure 2), since the silicate feature for this star appears to be self-absorbed, a sign that the optical depth near the peak is greater than unity. However, CIT 3 shows the same spectral changes as the optically thin sources, i.e. a relative enhancement near  $9.7\ \mu\text{m}$  during maximum. One could explain the spectral changes with the presence of additional dust condensing near minimum light causing the optical depth to increase, hence increasing the self-absorption. This is indeed a reasonable interpretation, however such a scenario is not plausible for the optically thin sources in our sample. Furthermore, NML Cyg has a mid-IR spectrum similar to CIT 3, but shows no variation whatsoever (see Figure 1). How can we explain this difference? This can be explained if CIT 3 is surrounded by a detached shell which is causing the silicate absorption feature. One can then hypothesize an inner dust shell, similar to IK Tau, internal to an optically thick “outer” shell, which causes the spectral line inversion. NML Cyg, on the other hand, has been recently modeled with an inner dust shell radius at approximately 12 stellar radii (Monnier et al. 1997). This distant dust will probably not experience grain formation and destruction during a pulsational cycle, since the grain temperature is less than 1000 K and gas densities are significantly lower. Additional mid-infrared and near-infrared interferometric observations could help resolve this issue.

### 3.2.4. *Dust Shell Heating and Cooling*

One other physical mechanism for causing a change in spectral shape as a function of luminosity is a change in the temperature. While the mid-infrared stellar spectral shape is relatively insensitive to changes in stellar effective temperature (Little-Marenin & Little 1990), the dust spectrum depends strongly on dust shell temperature because the peak of the Planck function lies within the mid-infrared for typical dust

temperatures, 500-1300 K. For optically thin dust envelopes following a radial, power-law density distribution, the radial temperature profile also follows a power-law relation from radiative transfer calculations. Hence, assuming no evolution of the optical constants themselves, changes in the spectral shape can be caused only by changes in the dust temperature at the dust shell's inner radius, not by changes in the optical depth or location of dust condensation, from self-similarity arguments (for recent discussion, see Ivezić & Elitzur 1997). Since the dust density distributions may be shell-like (from episodic mass ejection), consideration is also given to isothermal dust shell models. The effect of dust shell temperature variations on the spectral shape, as parameterized by the SP95 color-color diagram, can be significant. Figure 5 contains a curve which shows the effect on the spectral emission index for an isothermal shell at various temperatures (calculations for uniform outflow models show roughly the same magnitude of variation and are not included on the figure). Although a shell which evolves from 500 K at minimum to 1300 K at maximum almost matches the observed variations, such large changes are implausible from radiative transfer calculations and observations (typically  $\Delta T \lesssim 150$  K, Danchi et al. 1994).

It is quite plausible then that half of the spectral changes observed could be due to changes in the dust temperature, especially for cooler dust shells where the emission spectrum is more sensitive to temperature. However, reasonable physical constraints on the effective dust temperature and the plausible temperature variation exclude dust heating and cooling from being the sole explanation for the observed changes. This is especially true for U Ori, where the variations of the spectral shape of U Ori, especially near the peak, can be seen (Figure 4) to be too narrow to be caused by changes in the temperature alone.

### 3.2.5. *Changing Dust Properties*

Finally, the observed variability in the spectral emission index could be caused by changes in the dust optical constants themselves. This explanation has already been invoked to understand the narrow  $9.7 \mu\text{m}$  emission feature of U Ori, but may explain the overall shape changes as well. Dust grain absorption characteristics may be strongly dependent on the density and temperature of the ambient gas during grain formation. The adsorption of metal impurities onto the surface of grains as well as the development of amorphous dust grains during grain growth can have significant effects on the spectrum (cf. Tielens 1990; Stencl et al. 1990; Dominik et al. 1993). It is also known that grain size can affect the mid-IR emission spectra of warm dust grains, but this requires grains with radii larger than a micron (Papoular & Pegourie 1983). Such large grain sizes are typically not considered in preparing radiative transfer models, where conventionally the standard MRN dust grain size distribution ( $a < 0.25 \mu\text{m}$ ) observed in the ISM is utilized (Mathis, Rumpl, & Nordsieck 1977).

Theoretical studies of the nucleation of carbon grains (Fleischer, Gauger, & Sedlmayr 1992) indicate that dust formation is sensitively dependent on density and temperature, thus luminosity fluctuations or shock wave propagation can have unexpectedly large effects. Silicate grain formation theory is less well understood but efforts are presently underway to create a self-consistent, spherically symmetric model of the circumstellar environment of oxygen-rich miras, incorporating full radiative transfer, pulsation, and dust formation (Jeong et al. 1997).

### 3.2.6. Summary

In summary, a combination of dust shell temperature change and pulsational phase-dependent evolution of the dust grain characteristics can explain the observed spectral shape changes seen in Figure 2, while the production of especially “pure” silicate grains is likely required to explain the narrow ( $\Delta\lambda \approx 0.5 \mu\text{m}$ ) emission feature near the silicate peak during maximum light of a few stars. The general narrowing of the silicate peak, common to most of the stars in Figure 2, may be due to the evaporation of impurities from the grain surfaces or restructuring of the crystal lattice during re-heating preceding maximum light. Following maximum light, impurities adsorb onto the grains, broadening the solid-state resonance. More detailed laboratory measurements of astrophysically-realistic dust grains under varying physical conditions would be necessary to place the above scenario on firm physical footing. While the optical depth is expected to increase near minimum light as additional condensation occurs in the cooler circumstellar environment, this by itself should not strongly effect the shape of the dust spectrum if the dust optical properties remain fixed and the envelope remains optically thin, a condition met by most of the observed sources according to interferometric and spectral measurements.

### 3.3. Spectral Slope Changes or Enhanced Variability

Figure 3 presents the spectral monitoring of stars whose spectral shape showed either significant changes in slope or an rms shape variability larger than that expected from observations of standard stars. R Cnc and W Aql showed evidence of a shallower spectral slope during minimum luminosity than during maximum luminosity. Such a change in slope would be expected from heating and cooling of the dust shell. Indeed, simple calculations demonstrate that the observed changes are consistent with  $\Delta T_{\text{dust}} \approx 100 - 200 \text{ K}$  during the luminosity cycle and  $T_{\text{dust}} \approx 500 - 800 \text{ K}$ . A more detailed analysis can be done, but would require information regarding the geometry of the dust shell, e.g. the location of dust shell inner radius and dust density distribution.

IRC +10216 and R Leo are included in Figure 3 due to their large rms spectral shape fluctuations (IRC +10216 also shows weak evidence for a spectral slope change near maximum light). Such fluctuations may be indicative of a dynamic dust condensation zone, a zone permeated with atmospheric shocks and subject to chaotic dust formation/destruction processes. Alternatively, these fluctuations may be simply due to a relatively poorer calibration for these sources than the rest of the data sample. CIT 6 and V Hya (both carbon stars) also showed rms fluctuations somewhat above the average of  $\langle\sigma\rangle = 1.3\%$ , but these were not included here because they did not pass the  $\sigma > 2\%$  cut. Continued monitoring will be required to determine the true source of the observed changes.

## 4. Conclusions

The mid-infrared spectra of 30 late-type stars have been monitored in order to detect changes occurring on the pulsational time scale (typically 1-2 years) of long period variables (LPVs). Stars which exhibited little or no bolometric variability (i.e. non-LPVs) generally showed no change in their spectral shape in the range  $8\text{-}13 \mu\text{m}$ . Furthermore, most stars with no strong  $9.7 \mu\text{m}$  silicate feature, including carbon stars and oxygen-rich miras with broad, weak silicate features, showed no spectral shape change. However, a few such stars in this category displayed either enhanced variability as a function of wavelength (IRC +10216 and R Leo) or a detectable change in the spectral slope correlated with pulsational phase (R Cnc and W Aql).

The former effect has no clear explanation, while the latter effect can be explained by changes in the dust shell temperature ( $\Delta T_{\text{dust}} \lesssim 200 \text{ K}$ ).

The most significant result presented here is that nearly all of the observed sources with clear  $9.7 \mu\text{m}$  silicate features and definite bolometric variability showed strong evidence for changes in the silicate emission strength and spectral profile which are correlated with pulsational phase. We conclude that silicate emission variation is a general property of long-period variables with optically thin silicate features. The sharpening of the silicate feature near maximum light and its subsequent broadening can be explained by the heating and cooling of the dust envelope coupled with changing optical constants for the dust grains. The appearance of a spectrally narrow emission feature near the silicate peak of a few stars strongly indicates the existence of “pure” silicate dust grains near maximum light. We hypothesize that the general narrowing of the dust emission spectra may arise from pre-existing dirty grains whose surface impurities have been evaporated off or whose amorphous molecular configuration has crystallized during the dust re-heating following minimum luminosity. The solid-state resonance would naturally broaden after maximum light as impurities re-adsorb onto the cooled grain surface. Such speculation awaits more detailed laboratory measurements of astrophysically-relevant grain types.

The observations presented here remind us that the dust formation process is still only partially understood. Indeed, uncertainties in the optical constants for circumstellar dust are a primary obstacle in creating self-consistent multi-wavelength radiative transfer models incorporating interferometric observations of dusty objects (e.g., Monnier et al. 1997). The changes observed in silicate optical properties as a function of pulsational phase are not predicted by any present dust formation theories, and more careful consideration is required of the effects of photospheric shocks propagating into the dust formation zone and of the changing temperature and density structure due to the pulsation. Such models may then not only explain the changing optical properties of the dust around a single, pulsating object, but may also explain why different stars possess silicate emission with distinctly different spectral profiles.

The authors would like to thank Charles Townes, Peter Tuthill, Chris Matzner, and Irene Little-Marein for valuable comments. This research has made extensive use of the SIMBAD database, operated at CDS, Strasbourg, France. These observations were made as part of a long-term infrared stellar interferometry program at U.C. Berkeley, supported by the National Science Foundation (Grants AST-9315485, AST-9321289, & AST-9500525) and by the Office of Naval Research (OCNR N00014-89-J-1583 & FDN0014-96-1-0737). Some of these spectra were obtained as part of the UKIRT Service Programme. The United Kingdom Infrared Telescope is operated by the Joint Astronomy Centre on behalf of the U.K. Particle Physics and Research Council.

## REFERENCES

- Alksnis, A. 1995, *Baltic Astronomy*, 4, 79
- Bester, M., Danchi, W. C., Hale, D., Townes, C. H., Degiacomi, C. G., Mekarnia, D., & Geballe, T. R. 1996, *ApJ*, 463, 336
- Creech-Eakman, M. J., Stencel, R. E., Williams, W. J., & Klebe, D. I. 1997, *ApJ*, 477, 825
- Danchi, W. C., Bester, M., Degiacomi, C. G., Greenhill, L. J., & Townes, C. H. 1994, *AJ*, 107, 1469
- Dominik, C., Sedlmayr, E., & Gail, H. -P. 1993, *A&A*, 277, 578
- Draine, B. T. & Lee, H. M. 1984, *ApJ*, 285, 89
- Dyck, H. M., Benson, J. A., Howell, R. R., Joyce, R. R., & Leinert, C. 1991, *AJ*, 102, 200
- ESA 1997, *The Hipparcos Catalog (ESA SP-1200)*
- Fleischer, A. J., Gauger, A., & Sedlmayr, E. 1992, *A&A*, 266, 321
- Forrest, W. J., Gillett, F. C., & Stein, W. A. 1975, *ApJ*, 195, 423
- Goebel, J., Volk, K., Walker, H., Gerbault, F., Cheeseman, P., Self, M., Stutz, J., & Taylor, W. 1989, *A&A*, 222, L5
- IRAS Science Team. 1986, *A&AS*, 65, 607
- Ivezic, Z. & Elitzur, M. 1997, *MNRAS*, 287, 799
- Jeong, K. S., Winters, J. M., Fleischer, A. J., & Sedlmayr, E. in *Proc. A Half-Century of Stellar Pulsation Interpretations – Los Alamos, NM, USA, June 16-20, 1997*, in press
- Kukarkin, B. V., Kholopov, P. N., Pskovsky, Y. P., Efremov, Y. N., Kukarkina, N. P., Kurochkin, N. E., & Medvedeva, G. I. 1971, *General Catalog of Variable Stars (3rd ed)*
- Le Bertre, T. 1992, *A&AS*, 94, 377
- . 1993, *A&AS*, 97, 729
- Le Sidaner, P. & Le Bertre, T. 1996, *A&A*, 314, 896
- Little-Marenin, I. R. & Little, S. J. 1988, *ApJ*, 333, 305
- . 1990, *AJ*, 99, 1173
- Little-Marenin, I. R., Stencel, R. E., & Staley, S. B. 1996, *ApJ*, 467, 806
- Lockwood, G. W. & Wing, R. F. 1971, *ApJ*, 169, 63
- Marvel, K. B. 1996, New Mexico State University, PhD Dissertation
- Mathis, J. S., Rumpl, W., & Nordsieck, K. H. 1977, *ApJ*, 217, 425
- Mattei, J. A. 1995, private communication
- . 1997, *AAVSO Bulletin*
- Merrill, K. M. & Stein, W. A. 1976a, *PASP*, 88, 285
- . 1976b, *PASP*, 88, 294
- Monnier, J. D., Bester, M., Danchi, W. C., Johnson, M. A., Lipman, E. A., Townes, C. H., Tuthill, P. G., Geballe, T. R., Nishimoto, D., & Kervin, P. W. 1997, *ApJ*, 481, 420
- Morris, M. & Jura, M. 1983, *ApJ*, 267, 179
- Ossenkopf, V., Henning, T., & Mathis, J. S. 1992, *A&A*, 261, 567

- Onaka, T., de Jong, T., & Willems, F. J. 1989, *A&AS*, 81, 261
- Papoular, R. & Pegourie, B. 1983, *A&A*, 128, 335
- Sloan, G. C. & Price, S. D. 1995, *ApJ*, 451, 758
- Stencel, R. E., Nuth, J. A., Little-Marenin, I. R., & Little, S. J. 1990, *ApJ*, 350, L45
- Tielens, A. G. G. M. 1990, in “From Miras to PN: Which path for Stellar Evolution?” ed. M. -O. Mennessier (Editions Frontieres), 186
- Vardya, M. S. 1988, *A&AS*, 73, 181
- Wolf, N. J. & Ney, E. P. 1969, *ApJ*, 155, 181

Table 1. Journal of UKIRT Spectrophotometry

Date (U.T.)	Number of Spectra	Absolute Flux Calibration	Comments
1994 August 26	20	$\pm 5\%$	Cloudy for $\alpha$ Boo, RX Boo, $\alpha$ Sco, VX Sgr, $\delta$ Oph
1994 November 20	10	$\pm 20\%$	Not photometric
1995 January 14	19	$\pm 5\%$	
1995 March 17	24	$\pm 5\%$	Poor calibration for $9.7\ \mu\text{m}$ ozone line and band edges
1995 August 20	18	$\pm 10\%$	
1995 December 2	15	$\pm 10\%$	
1996 June 22	6	$\pm 15\%$	Patchy cirrus
1996 September 26	4	$\pm 5\%$	
1997 June 9	3	$\pm 10\%$	
1997 August 28	1	$\pm 10\%$	
1997 August 29	5	$\pm 5\%$	VX Sgr absolute calibration is uncertain

Table 2. Stellar Characteristics

Names	Spectral Type <sup>a</sup>	Variable Type <sup>a</sup>	Date of Maximum	Period (days)	# of Spectra	References
$\alpha$ Boo	K1.5III				4	
$\alpha$ Her	M5				3	
$\alpha$ Ori	M1.5Iab	SRc		~2070	7	1
$\alpha$ Sco	M1.5Ib	SRa		~1733	3	1
$\alpha$ Tau	K5III				6	
$\beta$ Peg	M2.5II-III				1	
$\chi$ Cyg	S8,K0III	Mira	2448688.5	402.3	4	2
CIT 3=WX Psc=IRC+10011	M9	Mira	2446985	660	7	5
CIT 6=RW LMi=IRC+30219	C	Mira	2449857	628	4	6
Egg Nebula=AFGL 2688	F5Iae				1	
$\delta$ Oph	M0.5III				4	
g Her	M6III	SRb		~70	4	1
IK Tau=IRC+10050	M6me	Mira	2447412	462	8	5
IRC+10216=CW Leo	C	Mira	2446825.0	638	5	3,4
IRC+10420=V1302 Aql	F8Ia				6	
NML Cyg=IRC+40448	MI <sup>b</sup>	SR		~940	5	7
<i>o</i> Cet=Mira	M7IIIe	Mira	2448826.3	333.8	7	2
R Aqr	M7IIIpe	Mira	2448619.9	383.9	3	2
R Cnc	M7IIIe	Mira	2448587.6	356.0	4	2
R Hya	M7IIIe	Mira	2448605.2	384	3	2
R Leo	M8IIIe	Mira	2448565.6	311.0	5	2
RX Boo	M7.5III	SRb	2449438	340	4	9
SW Vir=IRC+00230	M7III	SRb	2448637.12	153.6	2	2
U Her	M7III	Mira	2448652.8	418	1	2
U Ori	M8III	Mira	2448582.0	367	5	2
V Hya	C9	SRa	2447950	~529.2	4	1,9
VX Sgr	M4Iae	SRb	2448591	737	5	2
VY CMa	M5Iae	SR		~2000	4	8
W Aql	S4.9	Mira	2450762	490	3	10,11
W Hya	M8e	SRa	2448790.0	369	3	2

<sup>a</sup>From Simbad Database

<sup>b</sup>Supergiant classification based on Morris & Jura (1983)

References. — 1. Kukarkin et al. 1971; 2. ESA 1997 (Hipparcos Catalog); 3. Le Bertre 1992; 4. Dyck et al. 1991; 5. Le Bertre 1993; 6. Alksnis 1995; 7. Monnier et al. 1997; 8. Marvel 1996; 9. Mattei 1995; 10. Vardya 1988; 11. Mattei 1997.

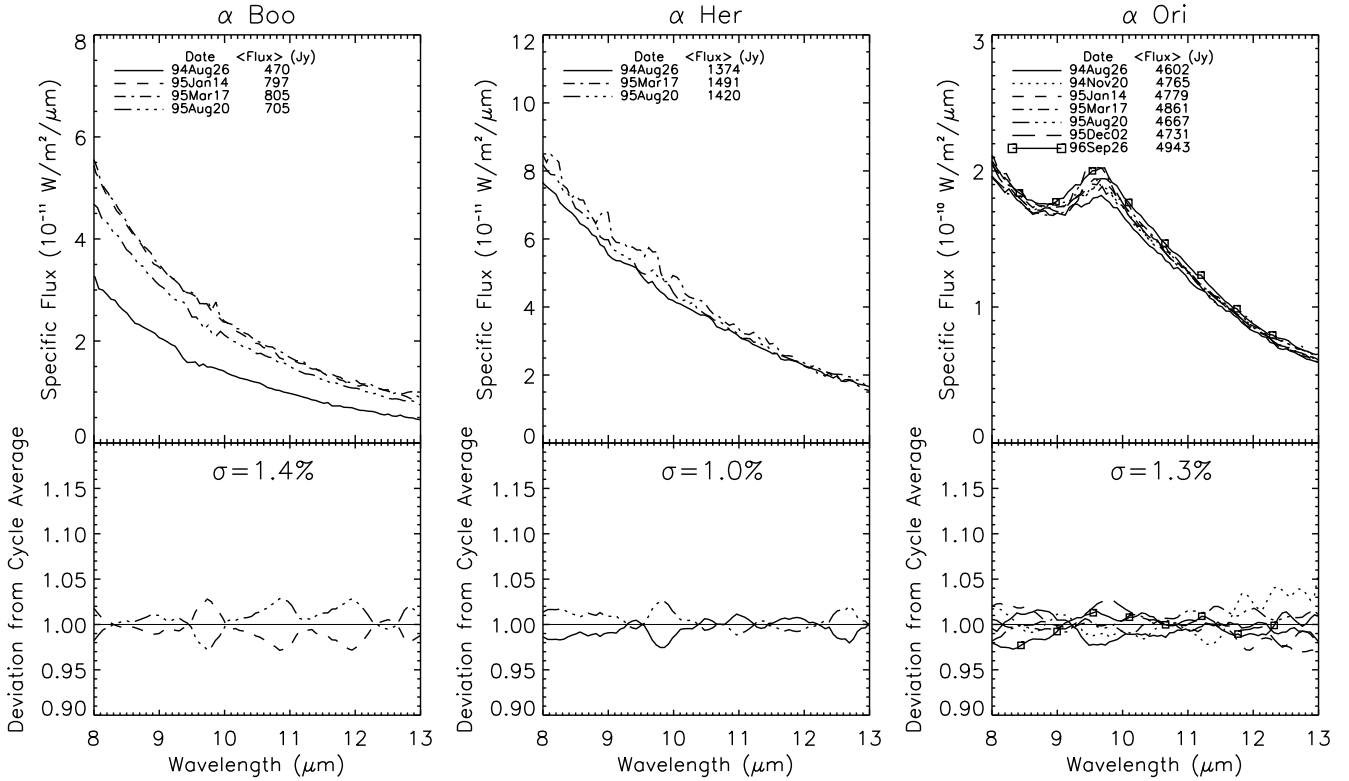


Fig. 1a.— Mid-infrared spectra of late-type stars which showed no apparent changes in shape (see §3.1). The top panels show the calibrated spectra along with the dates of observation, mean (8-13 μm) fluxes in Janskys, and the pulsational phases, if applicable. All spectra taken on a given date share a common linestyle to facilitate intercomparison. The bottom panels show each spectrum’s deviation from the cycle-averaged spectral shape, with the rms spectral shape deviation denoted by  $\sigma$  (see §3).

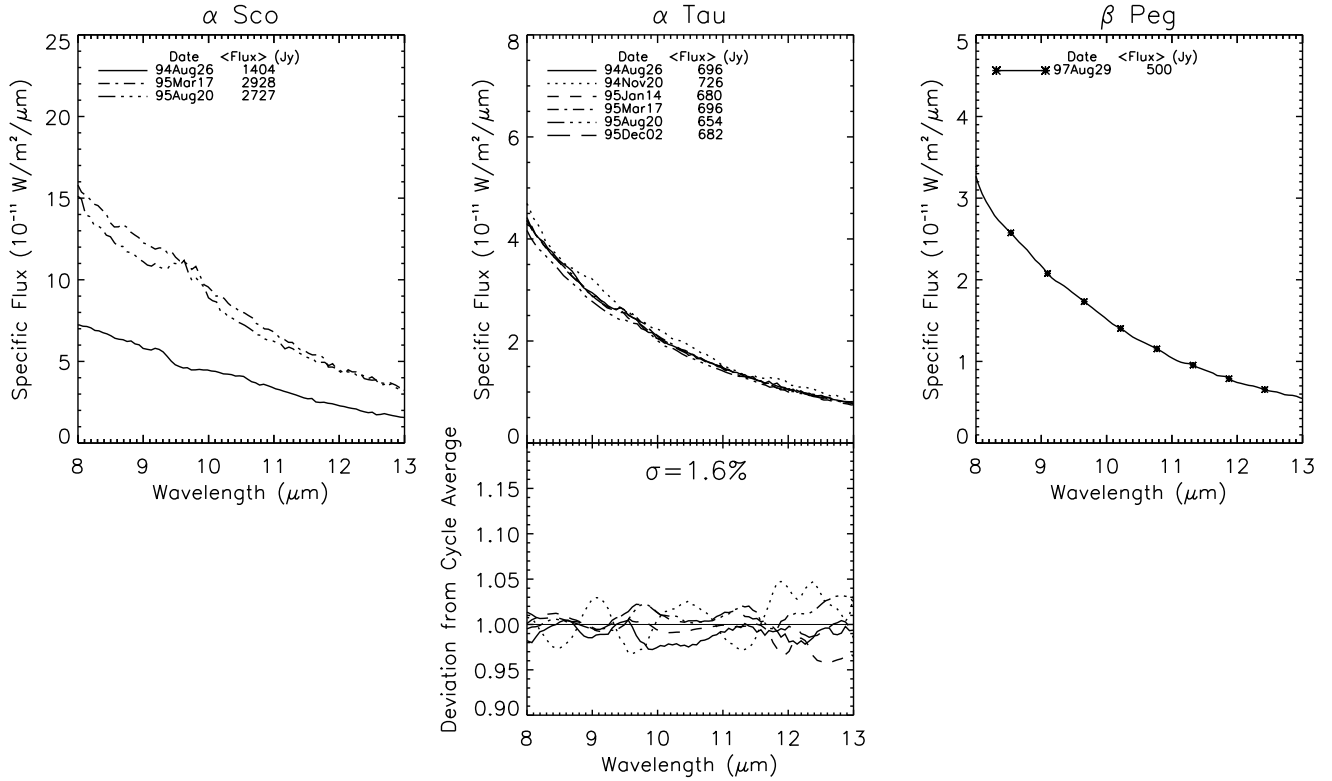


Fig. 1b.— Mid-infrared spectra of late-type stars which showed no apparent changes in shape (see §3.1). The top panels show the calibrated spectra along with the dates of observation, mean (8–13  $\mu\text{m}$ ) fluxes in Janskys, and the pulsational phases, if applicable. All spectra taken on a given date share a common linestyle to facilitate intercomparison. The bottom panels show each spectrum’s deviation from the cycle-averaged spectral shape, with the rms spectral shape deviation denoted by  $\sigma$  (see §3).

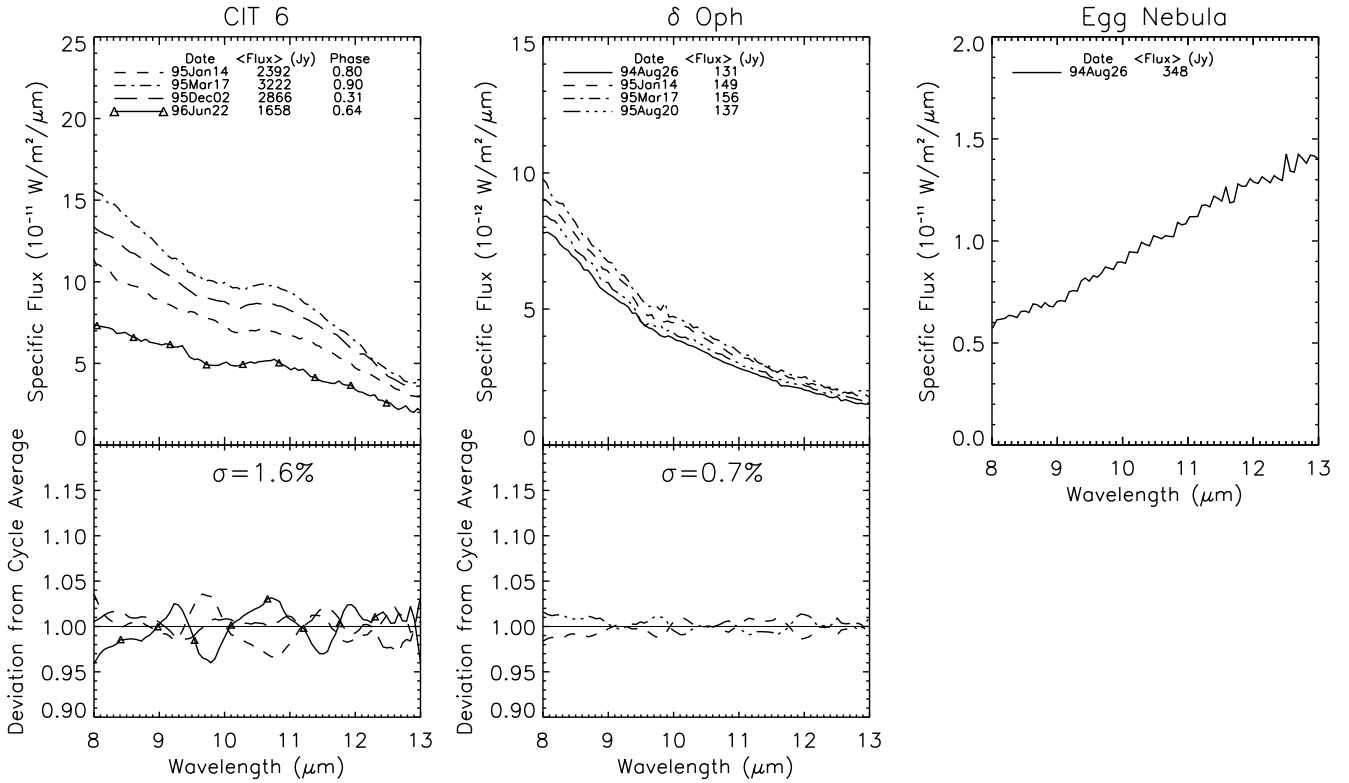


Fig. 1c.— Mid-infrared spectra of late-type stars which showed no apparent changes in shape (see §3.1). The top panels show the calibrated spectra along with the dates of observation, mean (8-13 μm) fluxes in Janskys, and the pulsational phases, if applicable. All spectra taken on a given date share a common linestyle to facilitate intercomparison. The bottom panels show each spectrum's deviation from the cycle-averaged spectral shape, with the rms spectral shape deviation denoted by  $\sigma$  (see §3).

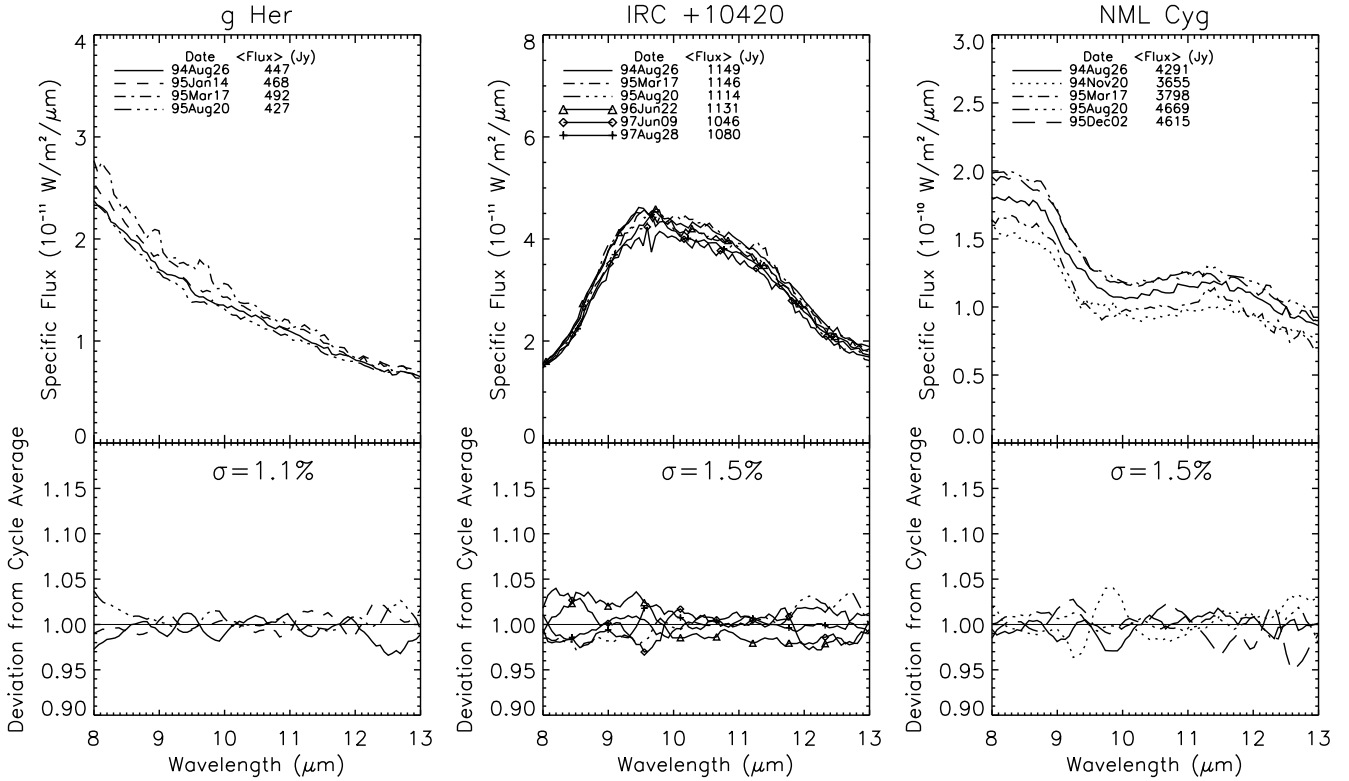


Fig. 1d.— Mid-infrared spectra of late-type stars which showed no apparent changes in shape (see §3.1). The top panels show the calibrated spectra along with the dates of observation, mean (8-13  $\mu\text{m}$ ) fluxes in Janskys, and the pulsational phases, if applicable. All spectra taken on a given date share a common linestyle to facilitate intercomparison. The bottom panels show each spectrum's deviation from the cycle-averaged spectral shape, with the rms spectral shape deviation denoted by  $\sigma$  (see §3).

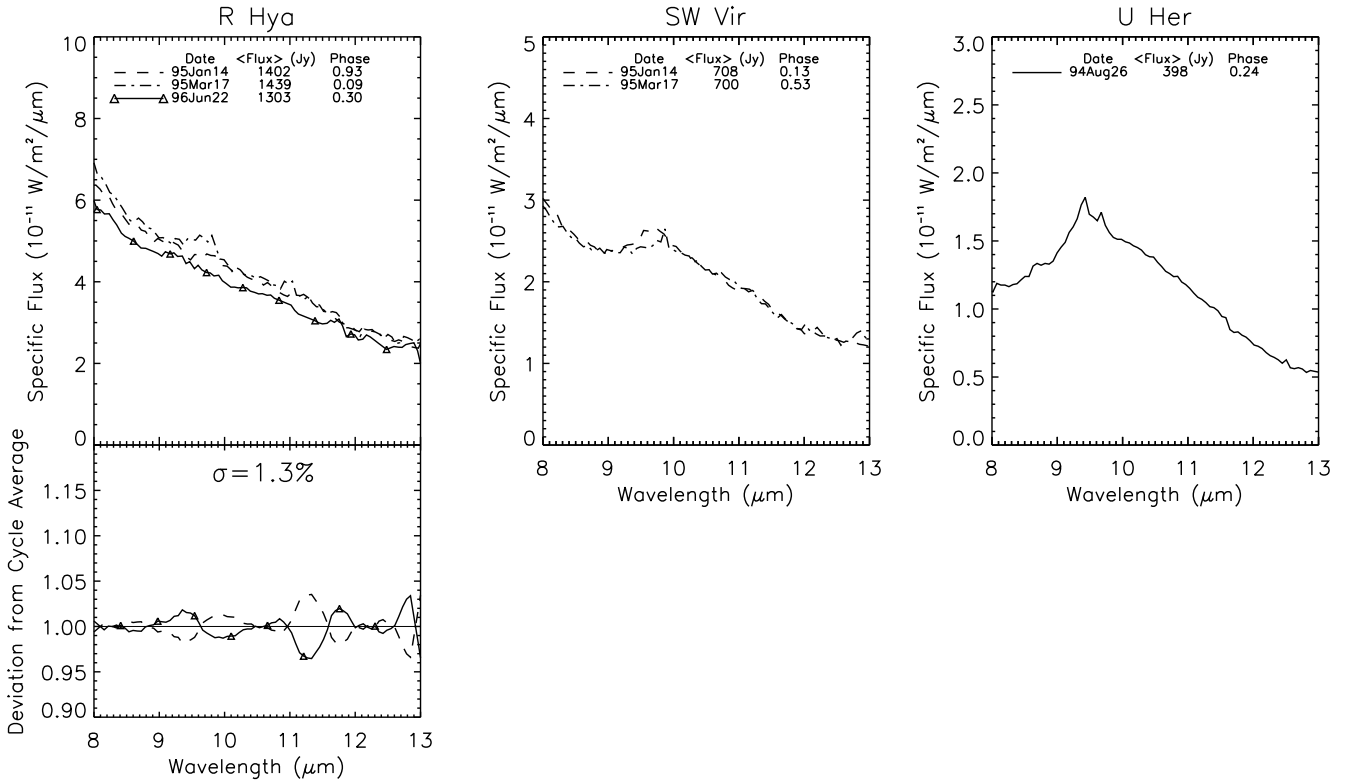


Fig. 1e.— Mid-infrared spectra of late-type stars which showed no apparent changes in shape (see §3.1). The top panels show the calibrated spectra along with the dates of observation, mean (8–13  $\mu\text{m}$ ) fluxes in Janskys, and the pulsational phases, if applicable. All spectra taken on a given date share a common linestyle to facilitate intercomparison. The bottom panels show each spectrum’s deviation from the cycle-averaged spectral shape, with the rms spectral shape deviation denoted by  $\sigma$  (see §3).

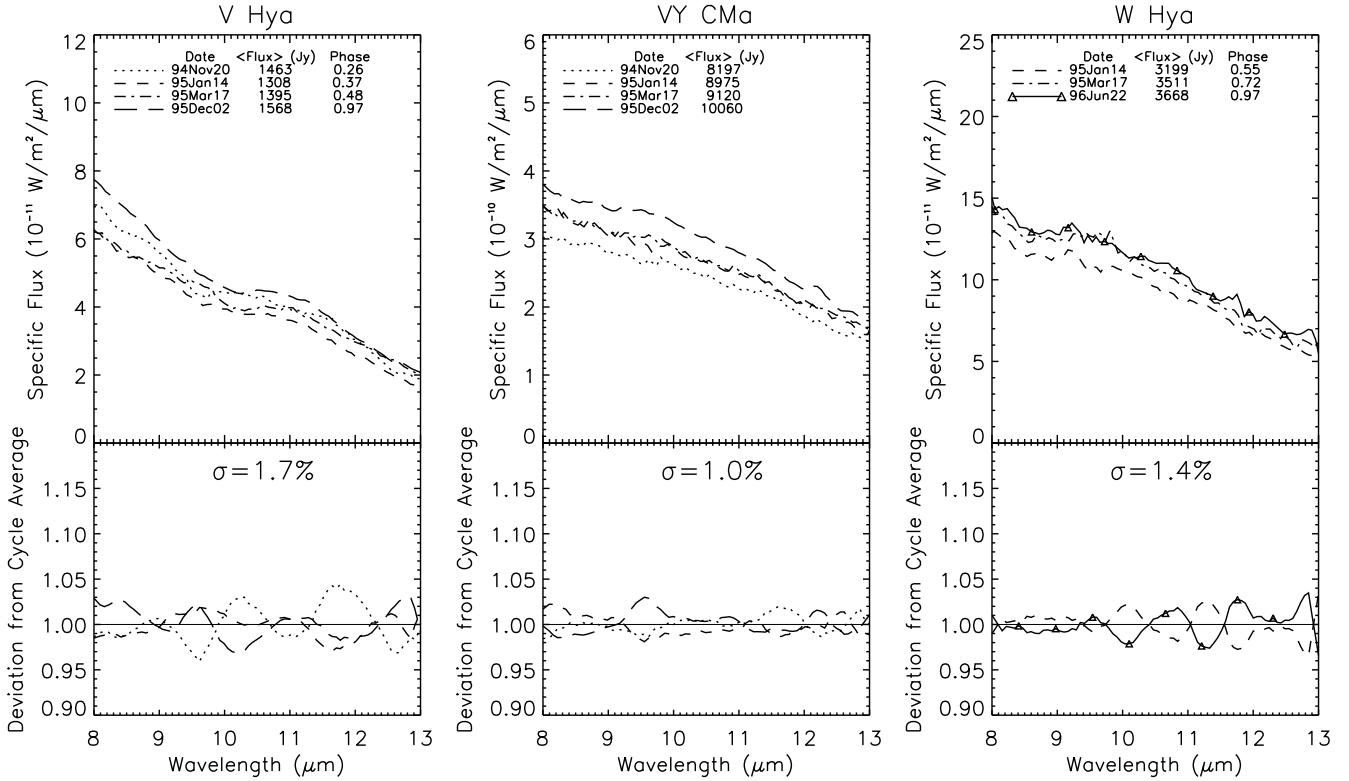


Fig. 1f.— Mid-infrared spectra of late-type stars which showed no apparent changes in shape (see §3.1). The top panels show the calibrated spectra along with the dates of observation, mean (8–13  $\mu\text{m}$ ) fluxes in Janskys, and the pulsational phases, if applicable. All spectra taken on a given date share a common linestyle to facilitate intercomparison. The bottom panels show each spectrum’s deviation from the cycle-averaged spectral shape, with the rms spectral shape deviation denoted by  $\sigma$  (see §3).

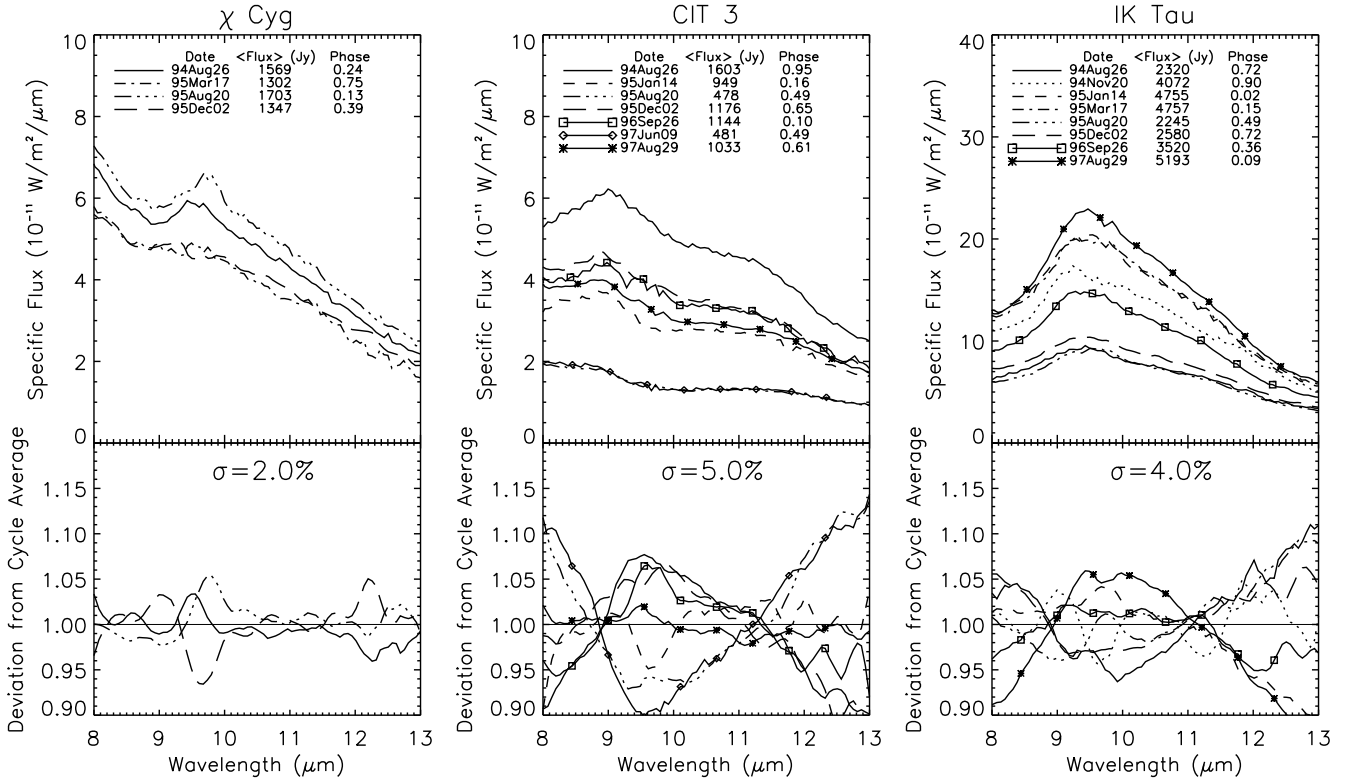


Fig. 2a.— Mid-infrared spectra of late-type stars whose silicate feature showed significant enhancement during maximum light (see §3.2). The top panels show the calibrated spectra along with the dates of observation, mean (8–13  $\mu\text{m}$ ) fluxes in Janskys, and the pulsational phases. All spectra taken on a given date share a common linestyle to facilitate intercomparison. The bottom panels show each spectrum’s deviation from the cycle-averaged spectral shape, with the rms spectral shape deviation denoted by  $\sigma$  (see §3).

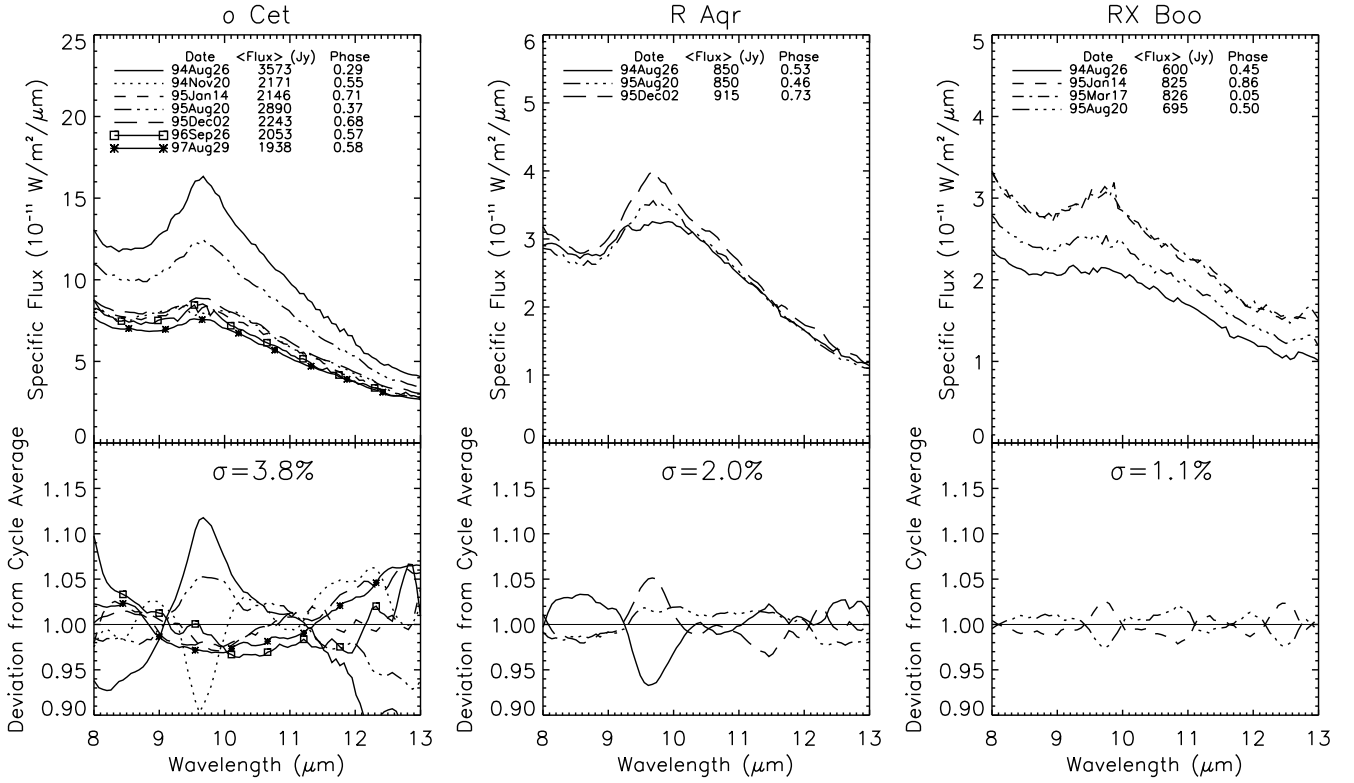


Fig. 2b.— Mid-infrared spectra of late-type stars whose silicate feature showed significant enhancement during maximum light (see §3.2). The top panels show the calibrated spectra along with the dates of observation, mean (8–13  $\mu\text{m}$ ) fluxes in Janskys, and the pulsational phases. All spectra taken on a given date share a common linestyle to facilitate intercomparison. The bottom panels show each spectrum’s deviation from the cycle-averaged spectral shape, with the rms spectral shape deviation denoted by  $\sigma$  (see §3).

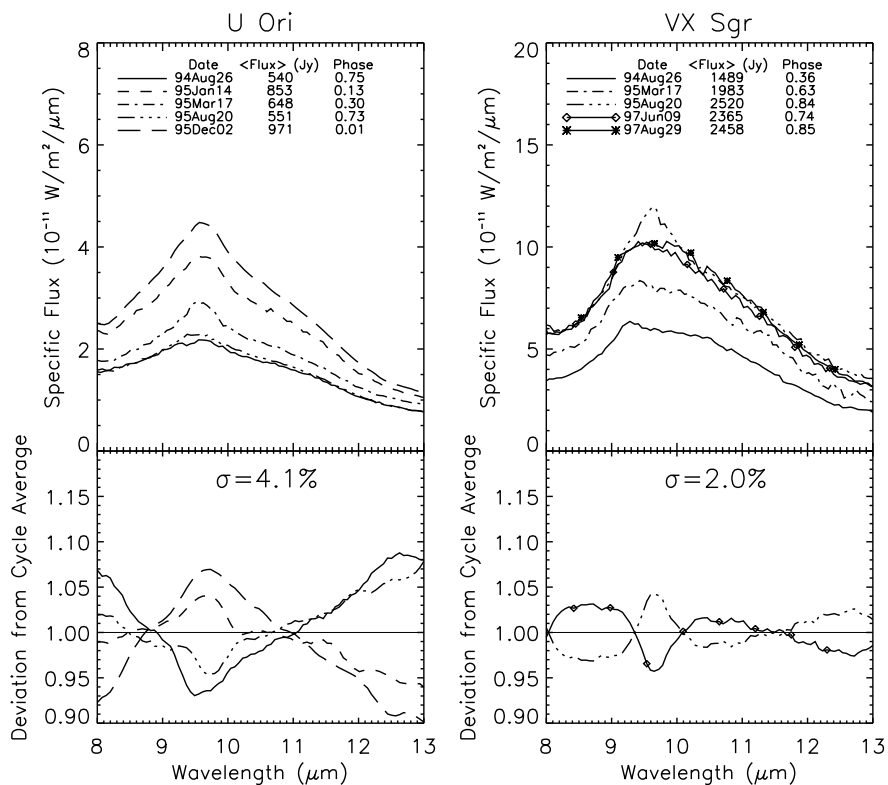


Fig. 2c.— Mid-infrared spectra of late-type stars whose silicate feature showed significant enhancement during maximum light (see §3.2). The top panels show the calibrated spectra along with the dates of observation, mean (8–13  $\mu\text{m}$ ) fluxes in Janskys, and the pulsational phases. All spectra taken on a given date share a common linestyle to facilitate intercomparison. The bottom panels show each spectrum’s deviation from the cycle-averaged spectral shape, with the rms spectral shape deviation denoted by  $\sigma$  (see §3).

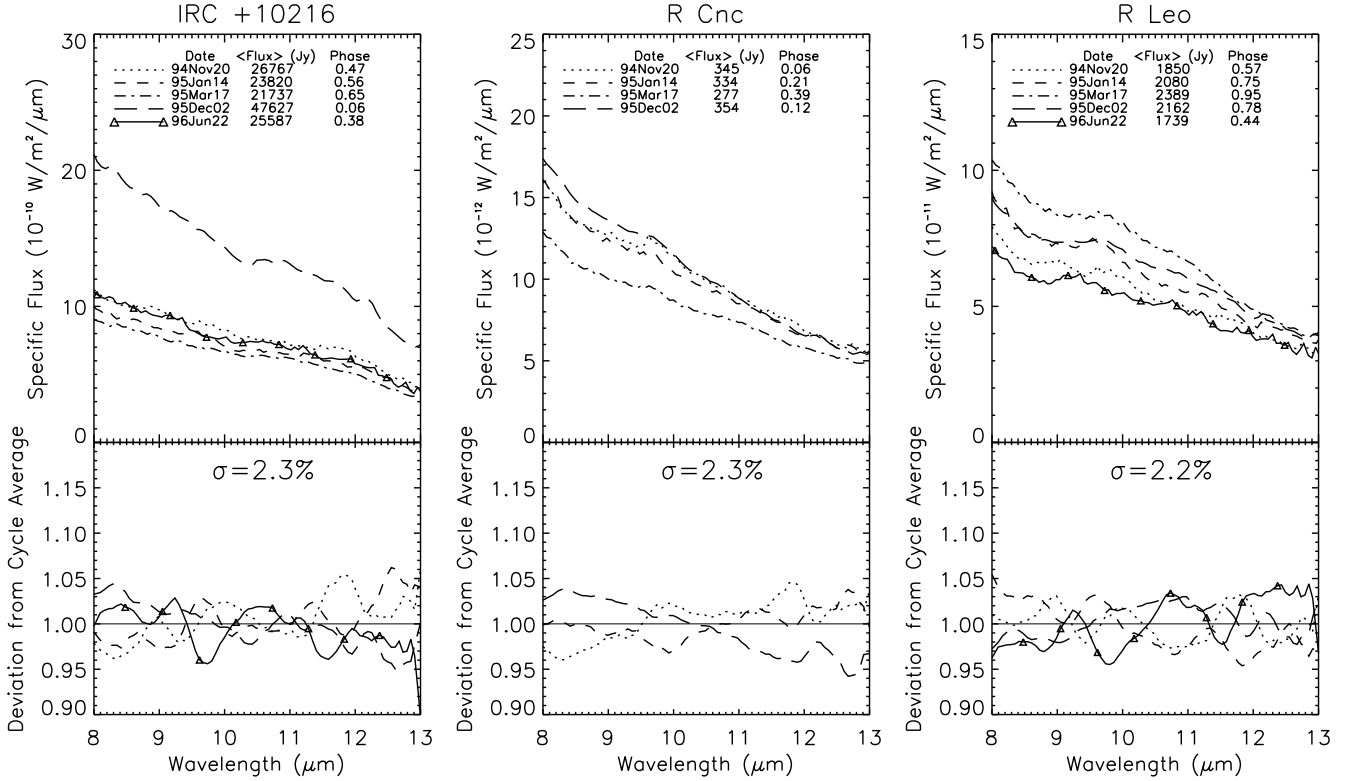


Fig. 3a.— Mid-infrared spectra of late-type stars which showed either significant changes in slope or an rms variability larger than that expected from observations of standard stars (see §3.3). The top panels show the calibrated spectra along with the dates of observation, mean (8–13 μm) fluxes in Janskys, and the pulsational phases. All spectra taken on a given date share a common linestyle to facilitate intercomparison. The bottom panels show each spectrum’s deviation from the cycle-averaged spectral shape, with the rms spectral shape deviation denoted by  $\sigma$  (see §3).

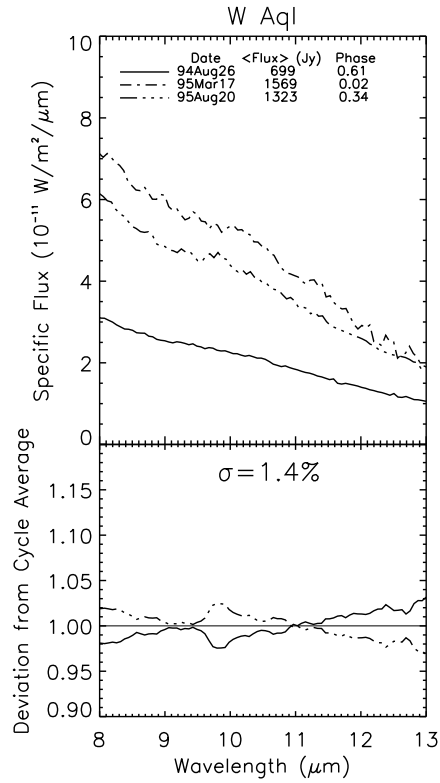


Fig. 3b.— Mid-infrared spectra of late-type stars which showed either significant changes in slope or an rms variability larger than that expected from observations of standard stars (see §3.3). The top panels show the calibrated spectra along with the dates of observation, mean (8-13  $\mu\text{m}$ ) fluxes in Janskys, and the pulsational phases. All spectra taken on a given date share a common linestyle to facilitate intercomparison. The bottom panels show each spectrum’s deviation from the cycle-averaged spectral shape, with the rms spectral shape deviation denoted by  $\sigma$  (see §3).

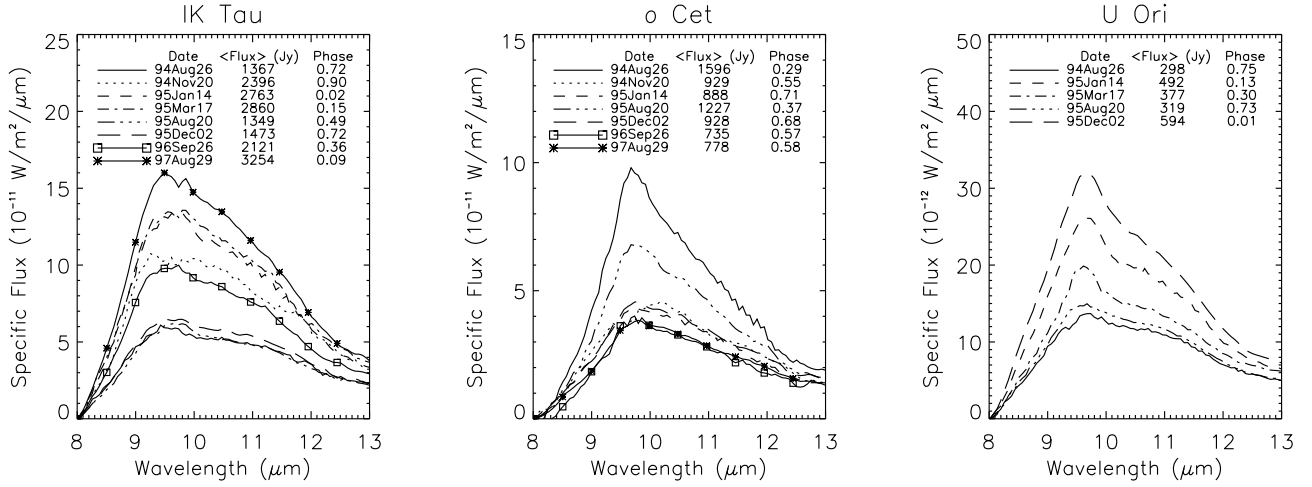


Fig. 4.— Stellar-subtracted, mid-infrared spectra of IK Tau, *o* Cet, and U Ori. By subtracting an estimate of the underlying stellar spectrum, changes in the dust spectrum itself can be more easily seen. Each panel includes a table containing the dates of observation, mean (8-13  $\mu\text{m}$ ) fluxes of the extracted dust spectra (in Janskys), and the pulsational phases. Note the prominent, narrow spectral feature near the silicate peak of U Ori which accompanies the star's rise towards maximum light (see §3.2).

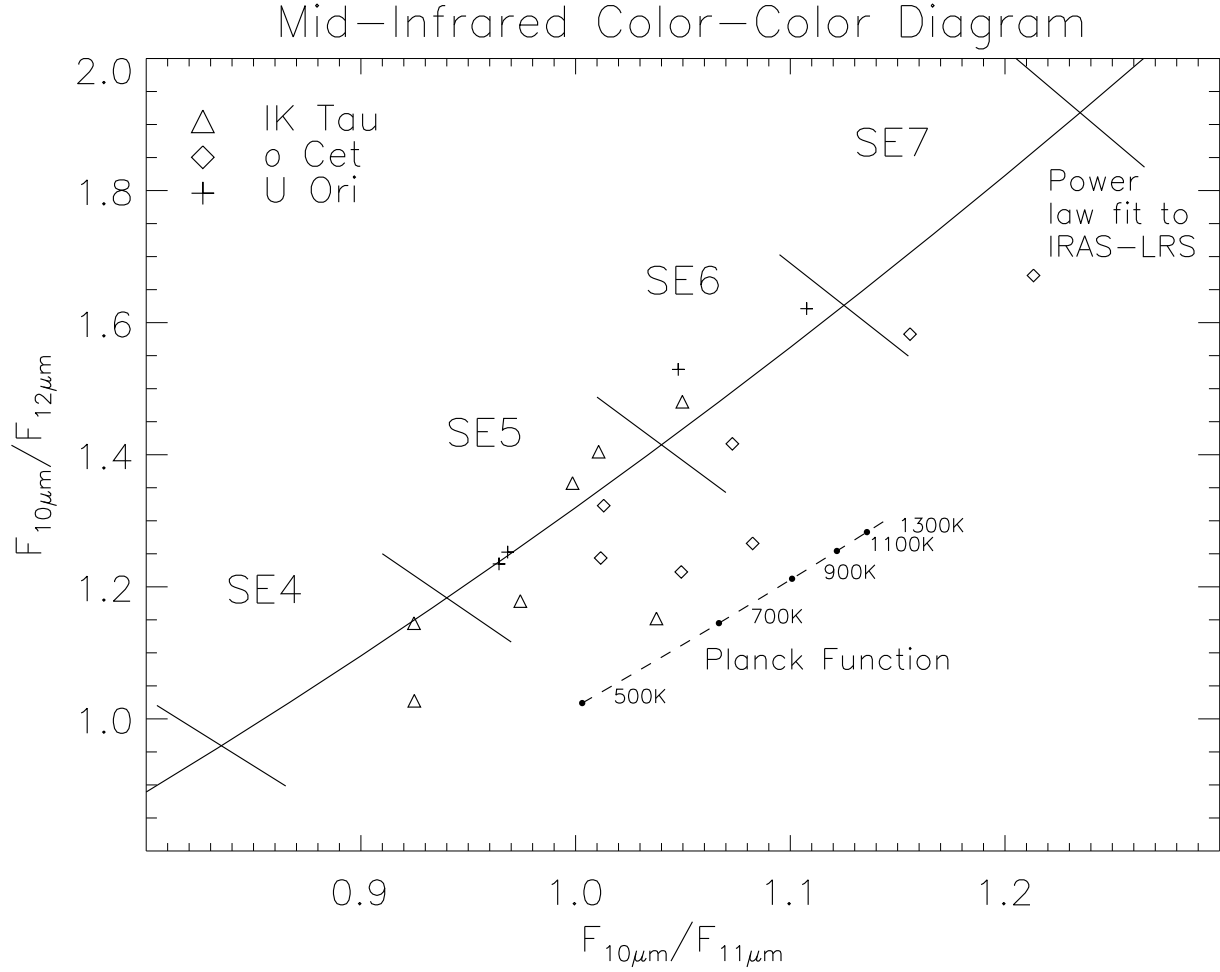


Fig. 5.— Color-color diagram for the evolution of the dust spectra of IK Tau, *o* Cet, and U Ori. Data points in the lower-left portion of the diagram represent stars near minimum light. The solid line is the power-law fit to the entire IRAS-LRS atlas performed by Sloan & Price (1995, SP95). The plot is divided into regions of similar spectral emission index (SE4-7) as defined by SP95, which parameterizes the narrowness of the silicate feature. The dashed line shows the effect of dust shell temperature changes on a given spectrum's location on this diagram. See §3.2 for more details.

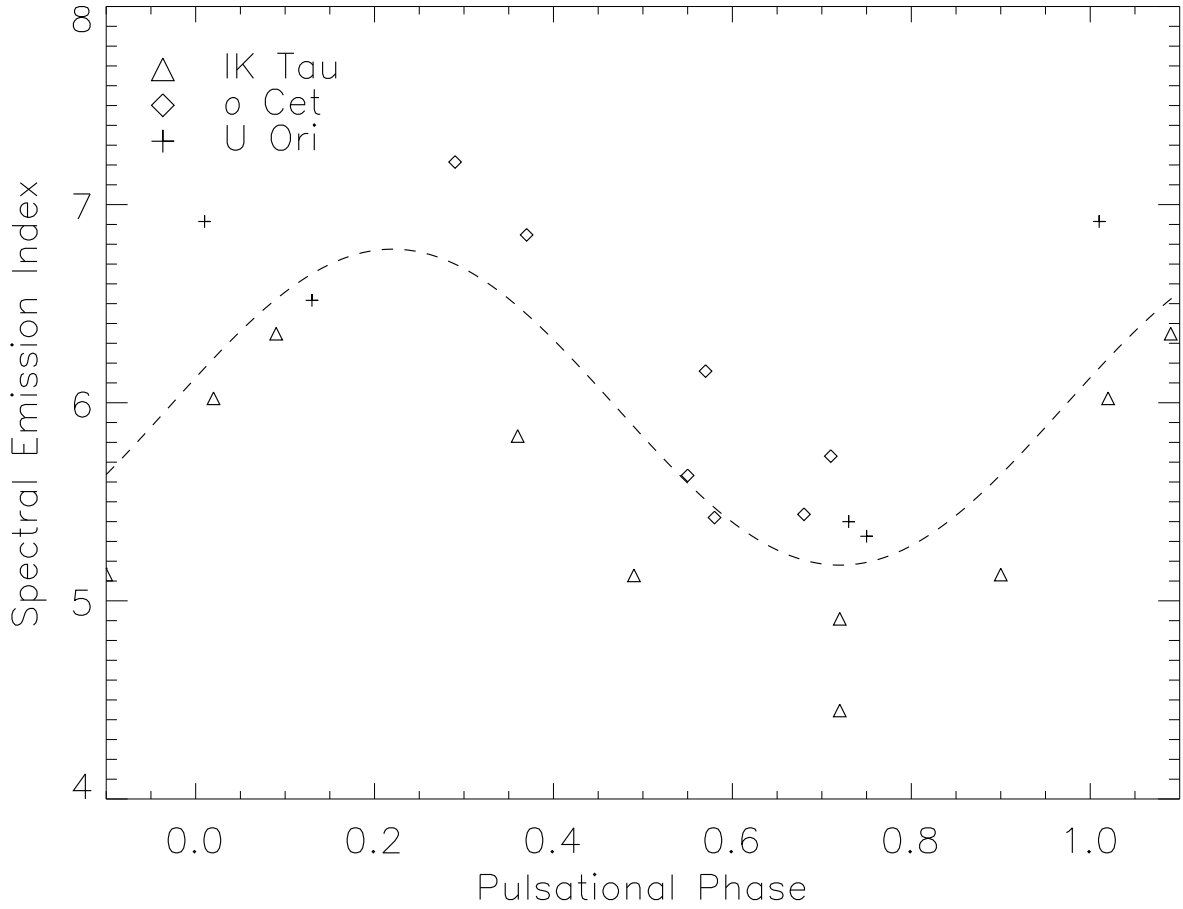


Fig. 6.— The spectral emission (SE) index as a function of pulsational phase for IK Tau, *o* Cet, and U Ori. These data were extracted from Figure 5 by projecting each spectrum’s location on the SP95 color-color diagram onto the power-law fit to the IRAS-LRS atlas. The SE index, which parameterizes the narrowness of the silicate feature, is seen to vary in phase with the pulsational cycle, reaching maximum values (sharpest silicate features) near maximum light. SP95 define the SE index as  $10(F_{11}/F_{12}) - 7.5$ . The dashed sinusoid is a rough fit to the data, included only to help guide the eye.